A Fixed-Wing Biplane MAV for Low Speed Missions

Chinnapat Thipyopas[1] and Jean-Marc Moschetta[2]
Department of Aerodynamics, Energetics and Propulsion
Institut Supérieur de l'Aéronautique et de l'Espace, University of Toulouse
31400 Toulouse, France
Chinnapat.Thipyopas@isae.fr, Jean-Marc.Moschetta@isae.fr

ABSTRACT

Practical MAVs missions, such as outdoor urban environment recognitions, simultaneously require a capability of both dashing to escape enemy fire and slowly loitering over a target in order to capture and transmit clear images to a ground station. Since an MAV intrinsically offers better payload and endurance capabilities than a rotorcraft of an equal size, fixed-wing MAVs can be considered as promising platforms to start with. The objective of this study is to investigate the possibility of developing a fixed-wing MAV which can both perform rapid translations and low-speed flights through urban canyons. A low-speed wind tunnel testing is conducted to compare several powered configurations including monoplane, biplane and tandem wing combinations. The testing also focuses on wing-propeller interactions. Results indicate that a positive-stagger biplane configuration powered by counter-rotating propellers placed in pusher position provides the best trade-off between a high-speed performance and a low-speed capability with a limited electric consumption. Consequently, a 30 cm-span MAV biplane prototype, named *TYTO-30*, has been designed and built. *TYTO-30* is equipped with a 110g-payload which includes a video camera, navigation and autopilot system and has been flight tested successfully.

NOMENCLATURE

ρ	Density
AoA	Angle of attack (deg)
Λ	Aspect ratio
B	Span
C	Chord
Cr	Chord ratio
C_D	Drag coefficient
C_{D0}	Minimum drag coefficient
C_L	Lift coefficient
D	Drag
I	Electric current (Amp)
K	Induced drag factor
l	Length
L	Lift force
L/D	Lift-to-drag ratio
M	Pitching moment
q	Dynamic pressure (Pa)
S	Surface
Sr	Surface ratio
T	Thrust
U	Velocity (m/s)
W	Weight (g)

[1]Research assistant, Department of Aerodynamics, Energetics and Propulsion, ISAE BP54032, 31055 Toulouse Cedex 4, France, chinnapat.thipyopas@isae.fr.

[2]Professor, Department of Aerodynamics, Energetics and Propulsion, ISAE BP54032, 31055 Toulouse Cedex 4, France, jean-marc.moschetta@isae.fr.

Subscripts

∞	Incoming freestream or Flight speed
α	Angle of attack
cg	Center of Gravity
LE	Leading edge
p	Propeller
R	Root chord
ref	Reference area/length
T	Tail
W	Wing

1. INTRODUCTION

Fixed-wing Micro Air Vehicles (MAVs) possess intrinsic capability to perform stable outdoor flights under windy conditions. They can be easily stabilized using miniaturized autopilot systems and have proved to be a reliable and robust solution to spot and identify a target from the sky.

Fixed-wing MAVs were first developed in the 1990s [1] and most configurations belonged to the low-aspect ratio monoplane wing category. This choice can be explained by the fact that MAV wings are subject to stringent constraints in terms of maximum overall dimension. It seems therefore desirable to occupy as much wing surface as possible and this low-aspect ratio wing results in very high induced drag. Due to the necessity to carry batteries, sensors, a navigation system and an automatic pilot, a fixed-wing MAV has to compensate its limited wing surface and low-aspect ratio wing with a fairly high cruise speed. As a consequence, fixed-wing MAVs may encounter difficulty to clearly capture stable images and adequately fulfil their surveillance mission.

An alternative to a fixed-wing MAV is a rotorcraft MAV. MAVs are ideally designed to perform hovering flights. However under windy conditions, they are practically more difficult to stabilize. Although recent MAV competitions such as MAV08 in Agra, India or EMAV 2008 in Braunschweig, Germany show that rotorcraft can actually perform quite well in outdoor conditions[3], rotorcraft endurance is generally limited and aerodynamic performance remains poor in forward flight.

Liu [2] has recently reported that birds use 26% less power than aircraft. Nevertheless, the maximum lift-to-drag ratio of scaled-down propeller-powered aircraft is around 11.9 while it is about 7.3 for birds. Therefore, when a video camera, an antenna and a fuselage are added, the flight efficiency of monoplane MAVs should not be expected to exceed 6–8 which is comparable to birds' efficiency [3–4]. Yet, flight mechanics and control of flapping vehicles remain poorly understood and it is very challenging to manufacture as the aeroelastic design and kinematic optimization of flapping-wings still require a lot of efforts [5–6].

The present study aims at designing a fixed-wing MAV configuration capable of low-speed phase and low drag. A typical surveillance mission consists of swiftly flying up to an observation zone and then slowly loitering over a target while transmitting clear images back to a ground station. It is assumed that covertness is a major concern and requires a capability of quickly dashing to the given remote zone.

2. FROM MONOPLANE TO BIPLANE MAV

It has been common a practice so far to retain monoplane wing configurations for the design of fixed-wing MAV prototypes. Monoplane wings are indeed more appropriate for heavy-loaded aerodynamic configurations and a highly constrained maximum size. They also offer an advantage of a relatively high maximum lift coefficient as a result of low aspect ratios.

At ISAE, we have designed and flight tested MAVs since 2000. The first generations were monoplanes, which also took part in the international MAV competitions. Section 2.1 briefly describes our best two candidates of the monoplane MAV prototype.

2.1. Starting with Monoplane MAVs

Monoplane fixed-wing MAVs have been developed for almost twenty years and most of them have been designed with a very low aspect ratio wing and a single propeller in tractor configuration. At ISAE, from 2000 to 2003, two fixed-wing monoplane MAVs called the *MinusKiool* and the *Plaster* were developed and equipped with electric motors. These two MAVs were low aspect ratio monoplane

[3]See, for instance, www.asctec.de.

flying wing concept with maximum dimension of 22 and 26.5 cm respectively. Both wing designs were carried out by optimizing non-powered wing planforms using computations and wind tunnel tastings to maximize lift-to-drag ratios. Because of their tailless configuration, double camber airfoils were applied both to the *MinusKiool* and the *Plaster*.

The *MinusKiool* main wing had an aspect ratio of 1.44 with a root chord of 140 mm, a wing span of 190 mm and a total weight of 58 grams. The outer parts of the wing had a positive dihedral angle of 30º and a leading edge sweep angle of 22º. A double camber airfoil of 8% relative thickness was used in order to accommodate batteries and electronic equipments. The *Plaster* wing planform shape was formed by joining a half-ellipse and rounded-corner rectangle at the quarter chord. The wing root chord was 175 mm and the span was 250 mm so that the aspect ratio was 1.65. A ready-to-fly radio-controlled model of 62 grams was fabricated with a 5º of dihedral angle applied to the wing so as to improve lateral stability. Both MAVs were powered by a single brushless motor and a two-blade propeller placed in tractor configuration as shown in Thipyopas [7]. As expected, the low aspect ratio wings stalled at a fairly high angle of attack, displaying a nonlinear lift slope and producing fairly high induced drag coefficients [8]. In addition, the monoplane MAVs usually came along with very high wing loading due to a combination of heavy equipments to carry such as batteries, video camera and transmitter, and stringent constraints to maximize the overall dimensions. In order to avoid producing high drag at high angles of attack, they generally flew at speeds greater than or equal to 15 m/s with a limited capability to fly at reduced speed. In the case of the *MinusKiool*, an elastic launcher was required to reach this speed during the take-off.

The next generation of our MAVs incorporated automatic flight control. In 2003, the *Plaster* was scaled-up to carry autopilot and navigation system. A fuselage was also added to provide more space for carry system components. The new design was called *LadyBug*. The 47 cm-wing-span *LadyBug* took part in the 4th European Micro-UAV Meeting (EMAV 2003, Toulouse, France) and in the 6th European Micro Air Vehicle Conference and Flight Competition (EMAV 2006, Braunschweig, Germany).

However, during the development, we have found that monoplane MAVs had inadequate capability to recognition mission scenarios in which target capturing and identification require low minimum speeds. Even in recent MAV competitions, such as MAV07 in September 2007 in Toulouse, most fixed-wing MAVs encountered difficulty to achieve the “locate-and-identify” outdoor mission because of their excessive flight speed, preventing operators to spot the targets on their ground station screen. Furthermore, complex tasks which require maneuverability and low speed, such as flying through arches and dropping a sensor in a small designated area have proved very challenging for most fixed-wing configurations. Reaching very low flight speeds can be performed by considering helicopter-type configurations. While rotorcraft remains difficult to miniaturize and control, they also usually require more energy to dash or to perform long-endurance surveillance missions. Therefore in this paper, we aim at exploring the possibility of modifying fixed-wing configurations to extend their flight envelope, improve low speed aerodynamic performance and still maintain their ability to perform fast forward flights.

2.2. Biplane vs. Monoplane MAV Configurations

At the University of Arizona, past attempts to extend the flight envelope of fixed-wing MAVs consisted of continuously modifying the relative wing camber [4] to lower the minimum achievable speed. The resulting in-flight adaptive wing proved to allow for a significant extension of the flight envelope and to ensure low-speed phases when needed.

An alternative strategy was followed at ISAE, where the biplane concept was revisited and applied to the low-Reynolds regime and low-aspect ratio configurations. Initially, the idea was not to extend the flight envelope toward the low-speed regime but primarily to lower the induced drag usually associated to low-aspect ratio monoplane wings under stringent dimension constraints [9]. Comparison between monoplane and biplane-wing concepts as applied to MAV was first based on a theoretical approach. Prandtl’s biplane theory was used and corrected with skin friction drag in order to compare monoplane and biplane configurations producing the same lift force under the same maximum size constraint. The conclusion was that the cruise performance of a fixed-wing MAV could be indeed significantly improved at high wing loads by using a biplane wing configuration. According to Moschetta and Thipyopas [10], a biplane MAV configuration would perform better than monoplane wings in cruise conditions only when the speed and the overall size were low, and the MAV was heavily loaded, which is usually the case for practical micro air vehicles carrying sensors and navigation devices. The proposed condition for selecting a biplane concept as opposed to a monoplane wing was of the following form

$$\frac{V^7 B^7}{W^4 \Lambda} \leq C \tag{1}$$

where C was a constant of the order of 460 $m^6\ kg^{-4}$. Yet, the major benefit of biplane MAVs turned out to be their capability to produce higher maximum lift than monoplane MAVs of equal size and weight. As a consequence, biplane MAVs could be considered as good candidate for slow flight phases. Furthermore, the weight penalties for the biplane due to an additional wing and struts was evaluated to represent a total weight increase of 5% since the additional struts weight could be partially compensated by the increase in wing aspect ratio allowed by the biplane configuration [10].

Although biplane effect has been well documented since the pioneering work of Munk and Prandtl in the 1920s [11–12], the effects of biplane parameters in the low Reynolds regime still needed to be conducted for MAV applications. Extensive experimental studies have been carried out in a low speed wind tunnel in order to study the influence of three main geometrical parameters such as gap, stagger and wing relative angle, also called decalage angle. The results indicate that at identical weight, maximum size and flight speed typical of MAV outdoor missions, the biplane wing produces less induced drag than the monoplane wing. Although, according to Prandtl's biplane theory, increasing gap can help to reduce the negative aerodynamic interference between the two wings, it is not beneficial to choose a gap greater than a wing chord because of the additional structure drag penalty and the increase in maximum dimension. The study also reveals that a slightly positive wing stagger can dramatically enhance the lift-to-drag ratio and the maximum lift coefficient. Applying a small positive relative angle slightly increases the aerodynamic performance and can be helpful for balancing the longitudinal pitching moment by creating a nose-down pitching moment. In addition, when combined with a positive stagger, a positive decalage angle tends to lower the stall angle on the upper wing, providing additional stability at high angles of attack.

In order to augment aerodynamic performance of low-speed biplane MAV, there are other parameters for biplane concept which can be modified such as span and chord ratio [13] as well as dihedral angle. Optimizing biplane chord ratio and propulsion installation is particularly investigated in the present paper.

3. PRELIMINARY STUDIES ON A BIPLANE TANDEM MAV

Preliminary tests and studies of biplane configurations were performed at the mini-UAV scale (60 cm-maximum dimension) in order to assess the benefit of the biplane concept in the low-Reynolds regime. Section 3.1 describes a first series of wind tunnel tests carried out to compare the aerodynamic performances of the monoplane *MaxiKiool* and the biplane *Avilent* of equal size and weight. Section 3.2 investigates another geometrical parameter involved in biplane and tandem wing configurations: the upper wing and lower wing chord ratio.

3.1. Comparison of a Monoplane and a Biplane Mini-UAV

A first biplane mini-UAV prototype called *Avilent* was investigated in an open loop Eiffel-type wind tunnel called S4 with an elliptical test section of 3 m × 2 m and a contraction ratio of 5. A 6-component sting balance was used to measure aerodynamic forces and moments with a piloted arm that can combine pitch, roll and yaw angles so as to explore angles of attack and sideslip angles in the range –10º to 90º. The model had 480 mm-span, as shown mounted in the wind tunnel test section as in Fig. 1. Both wings were equipped with the low Reynolds number high lift 12%-thickness airfoil, S1223 designed by Michael Selig [14]. The vertical distance between wings was 172 mm. The upper wing had a rectangular central part of 240 mm in width and a chord of 250 mm. On either sides of that central part, two trapezoidal parts were added with a chord of 80 mm at the wing tips so that the upper wing had a straight leading edge. The lower wing had a central part of 240 mm in width and a root chord of 280 mm. Two trapezoidal parts were added on either sides with a dihedral angle of 20 degrees and a wing tip chord of 100 mm. A forward sweep angle of 9.5 degrees was set to the lateral parts of the lower wing. Finally, the lower wing was equipped with a 40-percent chord plain flap that could be deflected independently on each part. The tandem wing was made from composite material and the junction between wings was made of aluminum. The *Avilent* model was equipped with two brushless motors AXI2208/34. A positive decalage angle of 6 degrees between both wings was set in order to ensure a positive pitching moment with respect to the aerodynamic center.

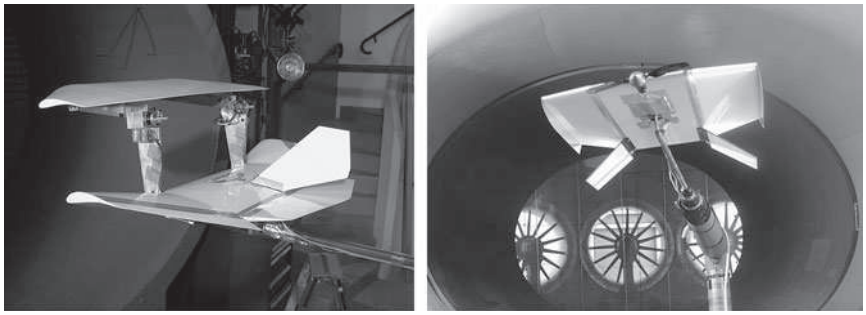

Figure 1. Avilent; Biplane MAV and MaxiKiool; Monoplane MAV.

The result from this test demonstrates that the propeller influence can actually increase the maximum lift coefficient especially at very low speed regime. Figure 2a illustrates the beneficial propulsive influence onto the lift coefficient at 4 m/s. The maximum lift coefficient of the present configuration increases from 1.3 (at an angle of attack of 25 degrees) to 3.8 (at an angle of attack of 48 degrees) due to the propulsive effect. This result includes the projection of propulsive force and the effect of propulsive induced flow on the model. The drag polar curve in Fig. 2b shows the advantage of the biplane wing over the monoplane wing to yield high lift coefficients. The *MaxiKiool*, a 3 times scale-up of the *MinusKiool* monoplane MAV, is plotted along with *Avilent*. Both airplanes have the same maximum dimension and measurements are carried out in the same low-speed wind tunnel. Although the monoplane configuration has a lower minimum drag, the tandem wing capability to perform low-speed flights is significantly superior with only a slight decrease of the maximum lift-to-drag ratio. Table 1 shows the result for longitudinal equilibrium at different flight speeds. The experimental results show that the *Avilent* configuration has a capacity to fly at very low speed.

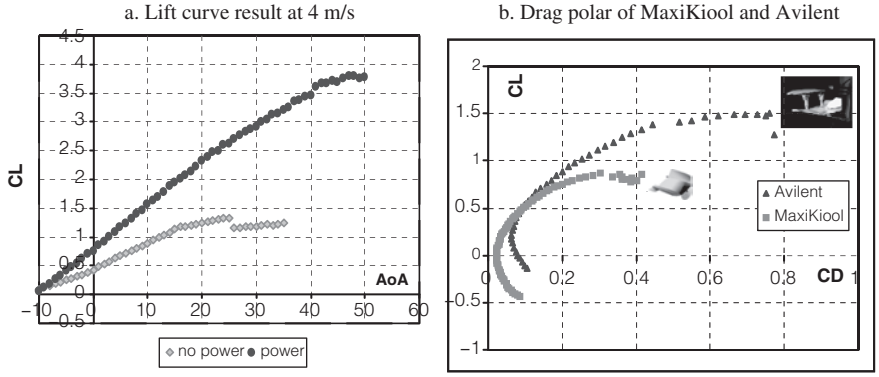

Figure 2. Lift characteristic and drag polar of Avilent.

Table 1. Wind tunnel result of Avilent

Speed (m/s)	Cl	Elevator Angle AoA (Deg)	Required Electric (Deg)	Power (W)
4	2.55	33.0	< –21	68.4
6	1.13	14.0	–6	45.6
8	0.64	3.0	2	35.3
10	0.41	–1.0	9	43.3
12	0.28	–3.5	10	62.7
14	0.21	–8.0	18	96.9
15	0.18	–9.0	19	114.0

In July 2005, a MAV prototype inspired from the *Avilent* wind tunnel model was fabricated and flight tested. In order to simplify the fabrication process, a 4%-camber curved plate profile was used along both wings and no dihedral angle was applied on either the upper wing or the lower wing. Two motors were located along the upper wing trailing edge as mounted on the *Avilent*. During the first flight test, the centre of gravity was placed between both wings and below the thrust axis. Due to that location, every change in thrust T created a spurious nose-down pitching M at the center of gravity which made the prototype difficult to manually control since

$$\frac{\partial M}{\partial T} < 0 \tag{2}$$

It was then decided to shift the center of gravity closer to the upper wing that it is to the thrust axis. The flight test showed that, in terms of longitudinal stability, it was much easier for a human pilot to control, but it had then poor lateral stability because of the center of gravity located on the upper wing.

3.2. Wing Chord Ratio Optimization Using VLM

The three classical biplane parameters: gap, stagger, and decalage angle, were study in previous studies. In the present section, the effect of an additional biplane parameter, namely the ratio *Cr* of the upper and lower wing chords, has been analyzed using a numerical simplified method and low-speed experimental measurements. The vortex lattice method (VLM) is used in this study to assess the effect of *Cr* at cruise conditions (i.e. at low angle of attack). The code TORNADO of Melin [15] has been modified to include viscous effects as described in [10]. The propeller-induced flow is not taken in account in the calculation although it has very strong effect on the aerodynamic performance of the low-speed biplane configuration. This is quite acceptable since the calculation is evaluated for a cruise condition which corresponds to at low incidence and a flow-field about the vehicle mainly dominated by the incoming cruise speed.

Three tandem wing configurations of wing chord ratio *Cr* equal to 0.467, 0.69 and 1 are calculated so as to produce a given lift force of 720 grams in all speed regimes. All three configurations have an overall wing span of 600 mm, as for the original configuration *Avilent*. In all cases, a static margin of 5% is sought and the decalage angle is adjusted so that the pitching moment at the center of gravity is zero. Figures in Table 2 illustrate the configurations simulated by TORNADO code. Table 2 indicates that the drag force reaches a minimum at given lift, for the intermediate chord ratio *Cr* = 0.69. This minimum is still valid for flight speeds ranging from 5 to 15 m/s. Even if it is small, the present calculation shows that it is beneficial to slightly shorten the root chord of the upper wing and lengthen the root chord of the lower wing.

Table 2. Calculation result of modified chord ratio by VLM

		Avilent Configuration	**Modified 1**	**Modified 2**
		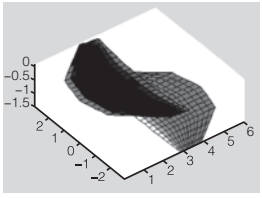	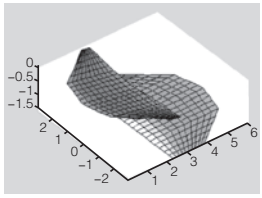	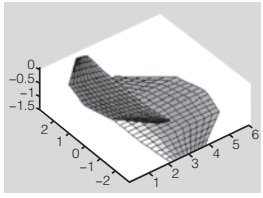
Chord Ratio		1.00	0.69	0.47
L/D at speed	5 m/s	3.29	3.46	3.36
	10 m/s	7.20	7.35	7.20
	15 m/s	6.05	6.86	6.67

4. BIPLANE AREA RATIO AND COMBINATION

Area ratio is another parameter that impacts aerodynamic performance of the biplane wing. Calculation in previous section and from literature reviews also lead to the same agreement. Although biplane arrangements had been previously investigated by identical biplane wing, biplane combination is performed again by unequal wing in this study.

4.1. Wind Tunnel and Micro Balance

All MAV models following this section were carefully tested in a closed-loop low-speed wind tunnel devoted to MAV studies at ISAE. The test section was 70 cm long with a square cross-sectional area of 45 × 45 cm^2. This wind tunnel had a contraction ratio of 6.2 and the flow speed could be adjusted by controlling the motor speed. A series of honeycomb grids at the beginning of the contraction cone gradually split and damped vortical structures so that the turbulence intensity of the incoming flow was reasonably low (~ 1%). In order to produce a stable and uniform flow at low speeds (2–3 m/s), the propellers pitch angle was reduced to 22º in the wind tunnel fan. Although the maximum speed was reduced from 40 to 20 m/s, stable speed regimes from 2 m/s to 20 m/s could be obtained with a standard deviation below 0.2 m/s. All powered models were measured using a new 5-component aerodynamic balance devoted to MAV studies [10]. The force measurements were accurate up to 0.4 grams or 0.004 N while the moments were accurate up to 0.2 gram-cm or 0.002 N.cm. The new balance was comparable to other aerodynamic balances specifically designed for MAVs [16–18]. The models were supported by three struts and inserted into the test section. The struts drag was carefully measured and corrected with the result of each observation. The test facility and the new balance are shown in Fig. 3 and described in [7, 10]. The uncertainty of low speed measurements were determined by combining the uncertainty of force and dynamics pressure measurements and the uncertainty of model dimensions. Aerodynamic characteristic uncertainties are shown in Table 3. The uncertainty on lift and drag presented in Table 3 was greater than the actual balance precision since the aerodynamic result must be further corrected by struts drag and model gravity effect.

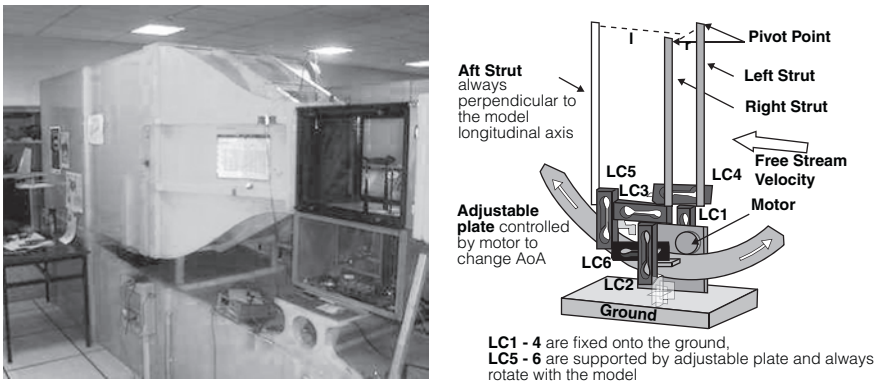

Figure 3. Low-speed wind tunnel and micro balance.

Table 3. Uncertainties of wind tunnel test at low speed

Velocity	Lift	Drag	Roll	Pitch	Yaw
5 m/s	0.9 g + 12%	0.3 g + 12%	2.0 g.cm + 2%	2.0 g.cm + 2%	2.0 g.cm + 2%
10 m/s	0.9 g + 5.6%	0.3 g + 5.6%	2.0 g.cm + 5.6%	2.0 g.cm + 5.6%	2.0 g.cm + 5.6%

4.2. Models

A series of wing planforms are shown on Fig. 4a and detailed in Table 4. All planforms are based on the Zimmermann planform, due to its high efficiency [8], but with varying aspect ratios. The Zimmermann planform is roughly equivalent to a combination of two half-elliptic forms in which the wing surface can be written as Eq. (3).

$$S = \frac{\pi\left(C_1 + C_2\right)B}{2} \tag{3}$$

where $C_1$and C_2 are secondary axis of ellipse 1 and 2 respectively, and b is the wing span.

All wing models fit into a 20 cm-diameter disk and are made of 2.5-mm thickness aluminium flat-plate. All edges are rounded with a radius of 1 mm. Several biplane MAV configurations have been built using different combinations of two selected wings chosen from Table 4 and connected by two aluminium struts of 4 mm thickness. The struts thickness is sufficient to provide enough rigidity to

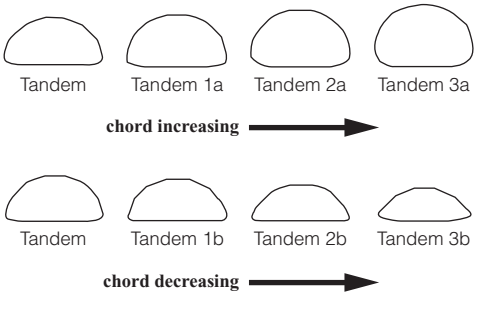

Modified Chord Wing Model

Tandem Configuration

Figure 4. Wing planform and biplane configuration.

Table 4. Wing models in chord ratio study

Wing Model		Surface Area (cm^2)	Wing Span (mm)	Λ	Wing Root Chord (mm)
Based	B	148.9	200	2.69	95
Modified 1a	M1a	168.5	200	2.37	105
Modified 1b	M1b	129.2	200	2.97	85
Modified 2a	M2a	187.5	200	2.13	115
Modified 2b	M2b	109.8	200	3.64	75
Modified 3a	M3a	208.0	200	1.92	125
Modified 3b	M3b	91.2	180	3.55	65

Table 5. Biplane chord ratio configurations and unpowered models results

Model	Lower Wing	Upper Wing	S_{total} cm^2	Sr	Cr	Stagger	L/D	CL_{MAX}	CL_A	CM_{AC}	AC_{LE}
Based	B (Z)	B (IZ)	298	1.00	1.00	> 0	4.08	0.82	2.46	0.003	61
Tandem1	*M1a (Z)*	*M1b (IZ)*	*298*	*0.77*	*0.81*	*> 0*	*4.12*	*0.88*	*2.40*	*0.008*	*59*
Tandem2	*M2a (Z)*	*M2b (IZ)*	*298*	*0.59*	*0.65*	*> 0*	*4.20*	*0.88*	*2.36*	*0.005*	*58*
Tandem3	*M3a (Z)*	*M3b (IZ)*	*299*	*0.44*	*0.52*	*> 0*	*4.19*	*0.90*	*2.19*	*0.006*	*54*
Tandem 1x	M1b (Z)	M1a (IZ)	298	1.30	1.24	> 0	4.25	0.85	2.41	0.007	63
Tandem 2x	M2b (Z)	M2a (IZ)	298	1.71	1.53	> 0	4.42	0.85	2.46	0.004	66
Tandem 3x	M3b (Z)	M3a (IZ)	299	2.28	1.92	> 0	4.42	0.86	2.35	0.006	64
Canard1	*B (Z)*	*M1b (IZ)*	*278*	*0.87*	*0.89*	*> 0*	*4.07*	*0.79*	*2.32*	*0.006*	*57*
Canard2	*B (Z)*	*M2b (IZ)*	*259*	*0.74*	*0.79*	*> 0*	*3.94*	*0.70*	*2.24*	*0.009*	*54*
Canard3	*B (Z)*	*M3b (IZ)*	*240*	*0.61*	*0.68*	*> 0*	*3.91*	*0.65*	*2.11*	*0.007*	*48*
Inverse Tandem 1	M1b (IZ)	M1a (Z)	298	1.30	1.24	< 0	4.04	0.55	2.40	0.007	56
Inverse Tandem 2	M2b (IZ)	M2a (Z)	298	1.71	1.53	< 0	4.23	0.57	2.34	0.007	56
Inverse Tandem 3	M3b (IZ)	M3a (Z)	299	2.28	1.92	< 0	4.45	0.67	2.16	–0.003	53
Biplane1	*M2b (IZ)*	*M2a (IZ)*	*298*	*1.71*	*1.53*	*→0*	*4.25*	*0.74*	*2.35*	*0.004*	*38*
Biplane2	*M2b (IZ)*	*M2a (IZ)*	*298*	*1.71*	*1.53*	*Low Positive*	*4.30*	*0.83*	*2.38*	*0.004*	*43*

Note: (Z) and (IZ) in 2nd – 3rd column represent wing planform; Aerodynamics coefficients are dimensionless by 20 cm-diameter disc area

damp vibrations during the propulsive tests. All tested models are described in Table 5, 1st – 7th columns. The root chord ratio and the surface ratio of both wings are defined by Eq. (4) and (5), respectively. For instance, if the upper wing has a surface lower than the lower wing, the area ratio is less than 1. From Eq. (3–5), then area ratio is equivalent to chord ratio in this study.

$$Cr = \frac{C_{R(upper)}}{C_{R(lower)}} \tag{4}$$

$$Sr = \frac{S_{upper}}{S_{lower}} \tag{5}$$

A positive stagger corresponds to the upper wing located upstream of the lower wing. The reduced stagger is calculated with respect to the lower wing chord. Three series of wing combinations called '*Tandem*', '*Canard*' and '*Conventional Biplane*' are of particular interest. The '*Tandem*' and '*Canard*' series have high stagger consisting of *Inverse Zimmermann* and *Zimmermann* wing for fore and aft wing respectively. All models of the '*Tandem*' series have the same total wing area while it is reduced for '*Canard*' configuration. The '*Conventional Biplane*' uses two Inverse *Zimmermann* wings and zero or low positive stagger are applied. Figure 4b illustrates the *Tandem1* configuration model in the test section. This photo was taken from the rear left side. All MAV models described in Table 5 were tested in the 45 cm × 45 cm wind tunnel at a freestream velocity of 10 m/s. The experiment was done for an angle of attack ranging from –5 to 30 degrees. In the absence of prop-wash effect, all biplane configurations typically stalled at an incidence of 15 to 20 degrees. When located along the upper wing trailing edge, propellers tended to delay the stall angle on both upper and lower wings [19].

In the following section, pitching moment coefficients are measured at 1 cm below the upper wing leading edge that is along the desired thrust axis. The aerodynamics center is assumed to be located along the propulsive axis and its longitudinal location is calculated from the evolution of the measured pitching moment as a function of the lift coefficient. One design constraint at a cruise speed of 10 m/s is to obtain a maximum lift force greater than 160 gram-force that is 2 times higher than the desired MAV weight. This factor 2 is selected to account for manoeuvrability.

4.3. RESULTS

Figure 5a shows the lift coefficient of a selection of biplane models as a function of the angle of attack. The lift coefficient of the monoplane wing *ZimA26* (Λ = 26) is also included for comparison. The tandem wings *(Tan & Tan2)* produce a maximum lift force of about 160 grams (C_L = 0.8) while other configurations only yield around 120 grams (C_L = 0.6). The canard (Car2) and the negative stagger tandem (Tan2SN) configurations produce lower maximum-lift-force than the tandem configurations. In the canard case, this is possibly due to the smaller total wing area. In the negative stagger case, this is the degradation of aft-wing performance at high angles of attack due to the forewing (or lower wing) wake. The drag of the different models appears to be only a function of the lift coefficient and does not significantly depend on the configuration itself. All pitching moment coefficients with respect to the aerodynamic center are very small because both wings use flat plate airfoils and no decalage angle is applied. Experimental results are also summarized in the 8th – 12th column of Table 5. The location of the aerodynamic center is defined from the fore-wing leading edge. In order to optimize the biplane performances as a function of the root chord ratio, a new scaling factor defined by Eq. (6) is used.

$$Cr' = Cr; \text{ if } Cr < 1 \quad \text{and} \quad Cr' = 1/Cr; \text{ if } Cr > 1 \tag{6}$$

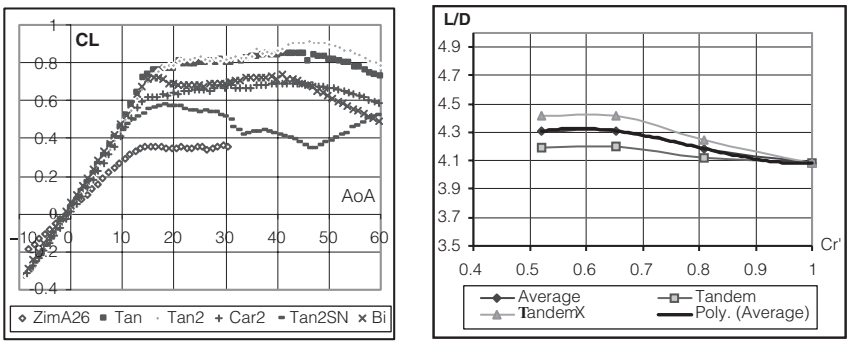

Lift coefficient of different configurations **Maximum lift-to-drag ratio vs chord ratio**

Figure 5. Unpowered biplane MAV result.

Figure 5b illustrates the maximum lift-to-drag ratio of "*Tandem*" and "*TandemX*" concept as a function of the reduced wing chord ratio *Cr*'. For a positive-stagger tandem wing, the combination of wing number 2 in configuration "*Tandem2*" and "*Tandem2X*" gives the best aerodynamic performance. The dark line represents the polynomial function of average value from both configurations and it can be written as a polynomial degree 3:

$$L/D = 7.445Cr'^3 - 17.628Cr'^2 + 12.997Cr' + 1.2666 \tag{7}$$

Experimental results show that the wing area-ratio is another important parameter and should be considered during a biplane wing optimizing design process. The derivative from equation (7) represents the optimized chord ratio, which can be obtained from

$$\frac{\partial\left(L/D\right)_{Cr'}}{\partial Cr'} = 0, \tag{8}$$

resulting

$$Cr' = 0.59 \quad \text{and} \quad Cr' = 0.99 \tag{9}$$

The biplane chord ratio, which gives the maximum lift-to-drag ratio, is around 0.6 for the *semi-Zimmerman* planform. This solution is consistent with the result obtained from the *VLM* calculation in Table 2. Then, cutting the monoplane wing into two *identical* smaller wings is not the best configuration that can be obtained at constant overall maximum dimension.

5. PROPULSIVE INTERACTION TEST AND RESULTS

In MAV configurations, the propwash effect is usually a dominant aerodynamic effect that significantly modifies the performance of the wing since the propeller diameter is comparable to the wing span. Furthermore at very low flight speeds, the velocity induced by the propeller tends to prevail over the incoming flow velocity. Therefore, it is essential to account for the prop wash effect when the propeller is placed in tractor configuration.

5.1. Experimental Setup

A new microbalance has been set up for propulsive-wing interaction tests as detailed in [7]. The propwash effect was investigated by performing several tests as illustrated in Fig.6. Wing models and propulsion sets were first separately tested in the wind test section while the angle of attack was varied, resulting in measurements denoted by *M(A)* and *M(P)* respectively. Then the interaction test, noted *M(I)*, was performed by placing both wing and propeller in the test section, each element being separately strut mounted without any physical connection. In order to confirm these tests, powered model measurements, noted *M(T)*, were carried out and compared with results of the interaction test. The propulsive strut drag, noted *Drag*, was carried out for the purpose of propulsive correction.

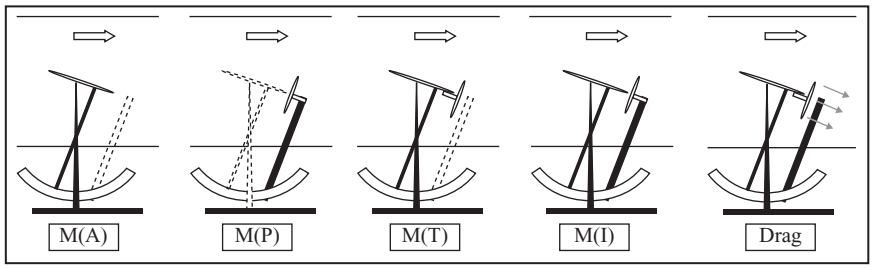

Figure 6. Interaction test setup.

On-board batteries were replaced by an external DC power supply limited to 11 volts, which corresponds to 3 elements of Lithium batteries. The motors used in this study were the brushless runner motor LRK 10-6-16Y, which weight only 6 grams. Each motor was mounted on a 5mm-diameter axis and was connected to a 3-gram speed controller YGE4-BL, connected outside the test section. The *Graupner*/JR *Quarz-Servo-Tester 764* was used to control the motor instead of the radio transmitter. The PWM (Pulse Width Modulation) signal from this device was sent to the speed controller. During the experiment, this device was control manually to maintain the electric motor consumption at a fixed desired value (5, 7.5 or 10 watts).

Table 6. Influent of propulsive induced flow on pusher and tractor monoplane wing

		Pusher Configuration			Tractor Configuration		
		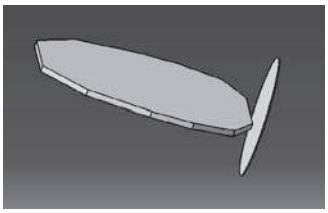			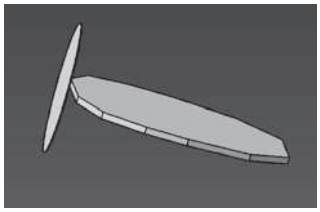		
	PWM	**CL_α**	**K**	**CD_0**	**CL_α**	**K**	**CD_0**
Wind Speed 5 m/s	0%	2.86	0.254	0.036	2.75	0.276	0.026
	50%	2.82	0.277	0.048	2.86	0.357	0.061
	100%	2.81	0.286	0.055	2.98	0.361	0.088
Wind Speed 10 m/s	0%	2.86	0.261	0.031	2.81	0.311	0.028
	50%	2.92	0.256	0.032	2.81	0.324	0.033
	100%	2.86	0.267	0.036	2.86	0.316	0.039

5.2. Propeller-Wing Interaction on a Monoplane MAV Configuration

The propeller-wing interaction was analyzed on a very low aspect ratio wing ($\Lambda = 1$), figure presented in Table 6). The comparison of pusher and tractor configurations shows that the aerodynamic characteristics of wing are highly influenced by the prop wash effect when the propeller is placed in tractor configuration. Both parasite and induced drag of the tractor configuration are dramatically higher than the pusher configuration due to the higher local speed and the modified local angle of attack in the propeller wake. Table 6 summarizes the wing aerodynamic characteristics influenced by the propulsive induced flow for both tractor and pusher configurations. At a low speed of 5m/s, the drag force is significantly increased in the case of a low-aspect ratio wing with a propeller in tractor configuration, which has been so far the standard configuration for fixed-wing monoplane MAVs. It has been observed that the propeller efficiency was not significantly affected by either tractor or pusher position up to an incidence of 30 degrees [20].

The propeller-wing interaction is further investigated for a higher aspect ratio wing. A Zimmermann wing of an aspect ratio of 2.13 with a thin camber airfoil NACA 4402 has been selected as a representation of the biplane configuration (Section 5.3). Several motor-propeller positions around the wing, as illustrated in Fig.7, are investigated in order to study the propeller-induced flow about the wing model. Positions no.1x–3x refer to the motor-propeller mounted at the wing trailing edge along a vertical plane. Position no. 1x corresponds to a propeller located under the wing lower surface while position no.3x corresponds to a propeller located above the wing upper surface. Positions no.2x and no.7x refer to the propeller placed on wing plane at wing trailing edge and the wing leading edge respectively. Positions no.4x–6x indicate a propeller placed on top of the wing upper surface. Different propeller positions along

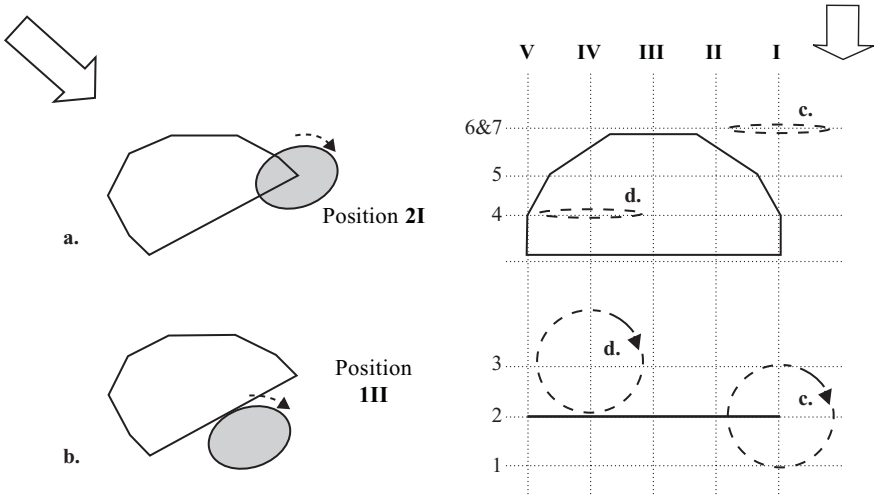

Figure 7. Propulsive induced flow test positions (on NACA 4402 wing).

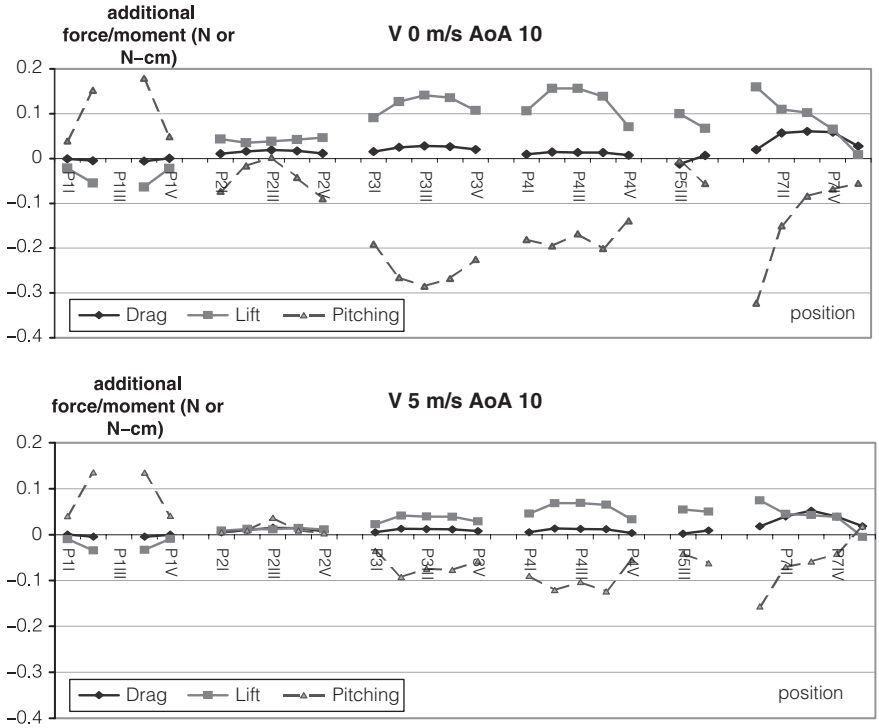

Figure 8. Propulsive induced flow on NACA 4402 wing model (α = 10 deg.).

the span wise direction, at mid span (III), quarter span (II) and wingtip (I), are also investigated. For positions I and V, clockwise or counterclockwise rotations are compared. In position I, the propeller rotates in the same direction as the wingtip vortex but in the opposite direction for position V. Results in Figure 8 concludes that mounting a propeller over the upper surface and behind the maximum camber position (positions no.3 & 4) produces the best performance. At that position, the increase in lift force is three times higher than the increase of drag force. On the contrary, position 1 (where the propeller is under the wing lower surface) logically degrades the lift force since static pressure is decreased. Although the experimental results indicate that the performance of position 7V, which corresponds to a set of tandem counter-rotating propellers counteracting the wing tip vortices as in the MITE [21] concept, it is not suitable to MAV configurations because of the increase of maximum dimension.

5.3. Propeller-Wing Interaction on a Biplane MAV Configuration

Different biplane configurations have been tested in a low-speed wind tunnel to investigate the values of gap, stagger, relative angle, chord ratio, and motor position that produce the best low-speeds aerodynamic performances. The study of biplane wing combinations reveals that, while using the same wing area, a positive stagger tandem wing configuration gives the highest maximum lift force. Another advantage of the tandem wing configuration is that the pitching moment at the aerodynamic center can be made positive by properly setting the relative angle between the upper and the lower wings without resorting to reflex airfoils. Cambered airfoils that produce higher maximum lift forces can then be used on both wings. Of particular interest is the question of the best location of propellers on a tandem-wing MAV. Because of a rapid dropping of propeller efficiency when its diameter reduces, the propeller usually represents a large portion of the wing span for the MAVs. In the case of the tandem wings in low-speed flights, it has been proposed to use a pair of counter-rotating propellers rather than a single propeller because of the limited amount of space available. Furthermore, counter-rotating propellers are beneficial to the vehicle control at low speeds where torque and gyroscopic effects become important. A series of six powered configurations illustrated in Fig.9 have been tested to explore the effect of combining a pair of propellers and a tandem wing configuration. In the tractor configuration, the propellers are placed at the upper wing leading edge and the blowing effect induced on the wing tends to delay the stall and to enhance flaps efficiency. However it adversely limits the achievable maximum-lift force. This is because the flow downstream the propeller disk is dominated by the induced velocity field and the local wing angle of attack remains small, even when the vehicle is placed at a high incidence with respect to the free stream velocity. Therefore the maximum

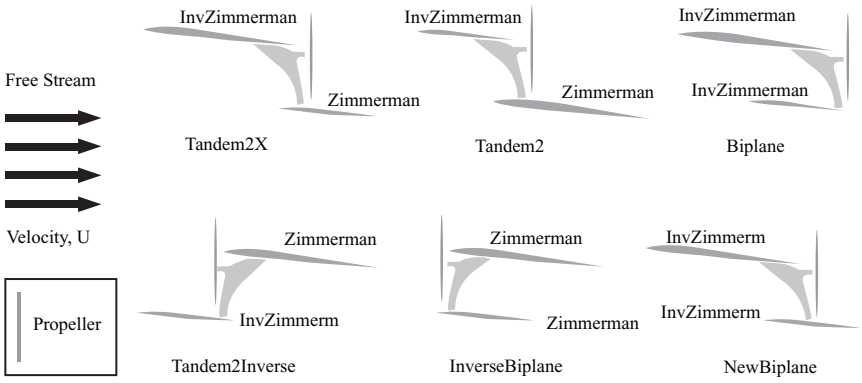

Figure 9. Tandem-wing MAV powered combinations.

lift force is limited. In the pusher configuration, the effective wing angle of attack is almost equal to the vehicle incidence. Therefore, higher maximum lift forces can be obtained on the wing even if the suction effect induced by the presence of the propeller along the trailing edge is limited.

In our wind tunnel testing the models are supported by three struts and inserted into the test section. The strut drag is carefully measured and corrected with the result of each observation. Since the effect of propellers is thought to delay stall, measurements are done at angles of attack ranging from –5 to 60 degrees, at a wind tunnel speed of 5 m/s (observation speed) and 10 m/s (cruise speed). Unfortunately, counter-rotating propellers of such small diameter are not currently available off the shelf. Two identical direct drive propellers GWS 3030, diameter 82 mm and pitch 7.6 mm, are used in this study. The propellers are mounted directly to the motor without any gear system. The experimental setup shown on Fig 10a is the '*Biplane*' configuration with two brushless motors and *GWS* 3030 propellers in the wind tunnel test section.

Table 7 shows, for a free stream velocity of 5 and 10 m/s respectively, the electrical current *I* (under a constant tension of 7 Volts) necessary to balance the MAV designed weight and the drag force. This electrical current is calculated by linear interpolation from a series of three powered tests

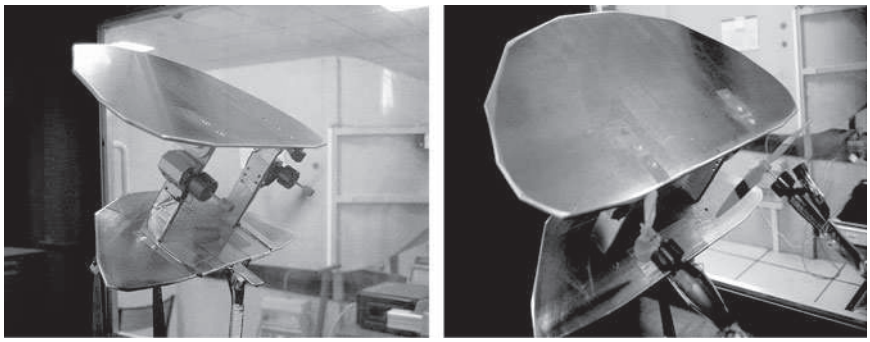

Figure 10. Biplane configuration; powered model (left) and propulsive-wing interaction test model (right).

Table 7. Results of powered model at low speed and cruising speed flight

	Velocity 5 m/s					**Velocity 10 m/s**				
	L=W, T=D				$\frac{L_{max}}{W}$	**L=W, T=D**				$\frac{L_{max}}{W}$
Model	**I; Amp**	**C_{MAC}**	**AC; cm**	**CL_{max}**		**I; Amp**	**C_{MAC}**	**AC; cm**	**CL_{max}**	
Tandem2	1.05	0.12	6.0	2.0	1.19	1.4	0.02	6.4	1.2	2.86
Tandem2X	1.4	–0.06	9.0	1.9	1.13	1.4	–0.02	7.5	1.3	3.09
Tandem2 Inv.	>1.5	0.03	4.0	1.4	0.83	1.05	0	5.0	1.0	2.38
Biplane	1	0.03	7.8	1.8	1.07	1.05	0.001	8.0	1.2	2.86
NewBiplane	1.05	–0.02	4.4	2.1	1.25	1.05	–0.02	5.1	1.35	3.21
Biplane Inv.	>1.50	0.04	2.2	1.6	0.95	1.05	0.005	2.6	0.9	2.14

at 5, 7.5 and 10 Watts. Table 7 also provides the ratio of the maximum lift force to the MAV weight at both speed regimes.

The results show that the '*Tandem2Inverse*' and the '*BiplaneInverse*' configurations in which the motors are mounted along the upper wing leading edge produce a lower maximum lift force than other configurations. They also require much electrical power to fly at low speed. This is due to the fact that the wing performance is reduced by the prop-wash angle when the wing is located downstream of the propellers. Although the '*Tandem2X*' gives the greatest lift force at high speed, it requires a fairly high electrical power. It seems that '*Tandem2*' and '*Biplane*' are good trade-off between a reasonable electrical consumption and a high maximum lift force. At the high angle of attack, the '*Tandem2*' configuration has a better performance in terms of maximum lift due to the effect of positive stagger as opposed to the low stagger '*Biplane*' configuration which results in spurious wake effects. However, the center of gravity of Tandem2 should be located on the small wing area where it is practically difficult to fit all the equipment. Finally, the '*NewBiplane*' configuration combines the best aspects of '*Tandem2*' and '*Biplane*' configurations and simultaneously provides a high maximum lift force and low electrical consumption.

The main drawback of the '*NewBiplane*' configuration is that the pitching moment coefficient is still negative (nose-down) at the aerodynamic center. Furthermore, since propellers are in a pusher configuration, virtually all aerodynamic efficiency is lost at low speeds. As a result, in order to design a flyable prototype based on the optimized '*NewBiplane*' configuration, a horizontal tail equipped with a pair of elevons has been added right after the propellers. With that horizontal stabilizer and the addition of a vertical junction at either tip of the wings, the *TYTO* configuration is designed to take advantage of the optimized tandem wing combination as described in section 6.

5.4. Comparison of Powered Biplane and Tandem MAV Configurations

The two configurations selected from the previous wind tunnel tests will be further examined in this section: the '*Biplane*' and '*Tandem2*' configurations, which provide respectively a high maximum lift and a low electrical consumption. The tests are performed at two freestream velocities, 5 and 10 m/s and at angles of attack ranging from –5 to 60 degrees. The first test is carried out without propeller installation and compared with a series of powered tests using 5, 7.5 and 10 Watts as in the previous section. In order to study the mutual interaction between the propeller and the wing model, two additional experiments are considered:

1) *Propulsion Test [M(P)]:* since the thrust is not constant when the angle of attack varies [22], the propulsion system is attached on an independent balance strut. The propulsive axial and normal forces without the presence of wings are measured at an angle of attack varying from –5 to 60 degrees. No moment measurements are measured on the propulsion strut.
2) *Propulsion-Wing interaction test [M(I)]:* as the second step, aerodynamic and propulsion forces are measured separately while the MAV model and its propulsion system are simultaneously present in the wind tunnel test section. The aerodynamic balance that supports the wing model measured force and moment coefficients. At the same time a separate balance measures the propulsion system, including both motors and propellers. The position of propeller is physically the same as in the global test *[M(T)]* of Section 5.3. As mentioned earlier, due to a low precision in the fabrication process, the relative position of the propellers with respect to the wings is not strictly independent on the angle of attack. Nevertheless, when the propeller is fixed in the wing trailing edge region, the relative location of the propeller turns out to have little effect on the global aerodynamic coefficients.

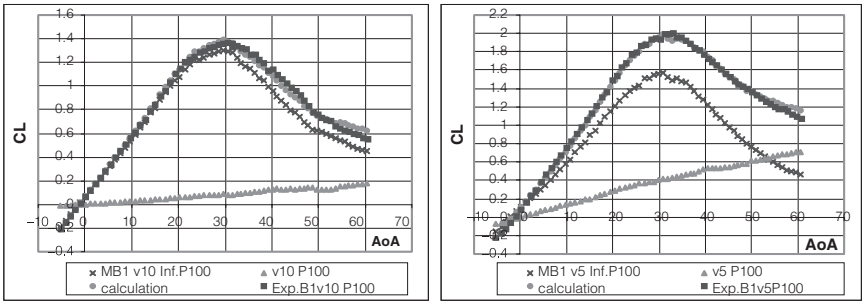

Biplane at high speed (10 m/s) *Biplane at low speed (5 m/s)*

Figure 11. Lift coefficients with/without prop-wash effects.

When summing the aerodynamic and propulsion forces, a global force is obtained. This force is very close to the experimental results presented in Section 5.3. The results are in good agreement at both high speed and low speed tests as shown in Figure 11 which compares the results from the global measurements *[M(T)]* and the calculation of Eq. 10. Bold black rectangular symbols represent the results obtained from section 5.3 where motors are attached on the wing model. Triangular symbols represent the propulsive force and "x" symbols represent the aerodynamic force acting on the model. Finally, the summation of both forces is represented by light gray circles. The discrepancy between the calculated lift coefficient and the global measurement may come from the slight relative position change at high angles of attack.

$$Force_{MAV}\left(calculated\right) = Force_{model}\left[M\left(A\right)\right] + Force_{propulsive}\left[M\left(P\right)\right] \tag{10}$$

$$Force_{MAV}\left(calculated\right) = Force_{MAV}\left[M\left(T\right)\right] \tag{11}$$

The propeller influence on wings can be analyzed by plotting the lift curves at different motor powers. The wings benefit from the propeller-induced flow especially near the stall at low Reynolds' numbers. At 5 m/s, the stall angle is delayed from 18 to 30 degrees due to propulsive effects as shown in Fig. 12a. The lift-to-drag ratio as plotted in Fig. 12b does not appear to be affected by the propellers influence, with an angle of attack corresponding to the maximum L/D close to 7 degrees.

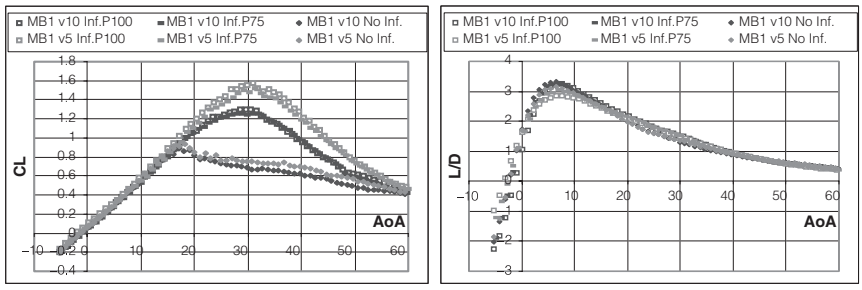

a: Lift coefficient *b: Lift-to-drag ratio*

Figure 12. Propulsive influence on the Biplane Model (black symbols = at v 10 m/s; gray symbols = at 5 m/s).

The thrust performance can be measured by comparing the propulsive forces with and without the model presence. The test is carried out by using the *Biplane* and *Tandem* configurations compared with propulsion-alone tests. At a speed of 10 m/s, no significant effects of *Tandem* and *Biplane* configurations are detected on the propulsive performance as opposed to a lower speed of 5 m/s. At low angle of attack, the influence of the model on the propulsion is very low for both configurations. In both cases, the presence of wings slightly decreases the thrust of propulsion system, particularly at angles of attack greater than 30º for which a wake effect occurs. At an angle of attack of 60º, the propulsive performance is decreased approximately 10% when the model is present. Yet, the trailing edge motor location still yields better a wing performance than the leading edge location.

6. DESIGN STRATEGY OF A LOW-SPEED BIPLANE MAV

Table 7 indicates a better efficiency of the *NewBiplane* configuration both in terms of maximum lift and of electric power requirement. In addition, one drawback of the *Tandem2* is that the upper wing chord is small and does not allow for much storage room. As a consequence, the *NewBiplane* configuration has been selected. Two motors are designed and placed at the trailing edge of the upper wing and over the lower wing at 40% chord line. Since the *NewBiplane* configuration is expected to achieve low minimum speeds, the longitudinal MAV control may be difficult if the propellers are placed in pusher configuration. In order to guarantee a sufficient aerodynamic efficiency over control surfaces at low speed, a horizontal stabilizer has been designed and placed right downstream of the propellers so as to benefit from the propeller-induced flow.

6.1. Tail Surface Design

The aerodynamic model obtained from the linear part of the wind tunnel result has been used to design the horizontal tail. The objective is to balance the prototype in level flight at a velocity of 10 m/s

($L = W$, $T = D$, and $M_{CG} = 0$). Because the propeller-induced flow dominates the flowfield in the wake at low speed, the flow downstream the propeller is highly modified both in direction and velocity. McCormick's method describing the flow field of a propeller slipstream has been considered in the present study [23]. However, McCormick analyzed the case of a propeller placed in a freestream flow which differs from the present propulsive pusher configuration. In the present approach, the incoming flow as seen by the horizontal tail is not considered to be the freestream velocity but a flow is assumed to be perpendicular to the propeller disc with a dynamic pressure over the tail greater than the dynamic pressure over the wing. That is consistent with the fact that the horizontal tail should be located very close to the propellers for compactness purpose. The momentum theory is applied to calculate the flow speed behind the propellers and the propulsive thrust. The tail preliminary design is based on a rectangular planform of aspect ratio 3. The aerodynamic characteristics of the tail are determined from the extrapolated value and the equation proposed by Mueller et al [8]. The lift, drag and pitching moment equation are formulated. The calculation is carried out by tried out and error by changing a velocity after the propeller and tail setting angle. Finally, the calculation results in a tail setting angle of –3 degrees with respect to the propeller axis and a rectangular planform of 9 × 3 cm^2. Table 8 summarizes the parameters and equations used in this calculation.

Table 8. Tail design modelling of TYTO

Wing Aero. Characteris Tics	**Aero. Coefficient**	**Force**	**Aero. Model**
$\alpha_{L=0}$	0	**Main Wing**	
C_{L_α}	0.0515 / deg	q_∞	$0.5\rho\left(U_\infty^2\right)$
C_{D0}	0.060	L	$0.5\rho\left(U_\infty^2\right)S_{ref}C_L$
K	0.001	D	$0.5\rho\left(U_\infty^2\right)S_{ref}C_D$
C_{M_α}	–0.0019 / deg	M_{cg}	$0.5\rho\left(U_\infty^2\right)S_{ref}\overline{C}_{ref}C_{M(cg)}$
$C_{M(ac)}$	0		
C_L	$C_{L\alpha}(\alpha)$	**Tail**	
C_D	$C_{D0} + K \cdot C_L^2$	q_T	$0.5\rho\left(V_p^2\right)$
$C_{M(cg)}$	$C_{M_\alpha}(\alpha) + C_L l_w$	L_T	$0.5\rho\left(V_p^2\right)S_{ref}C_{L(T)} \times \left(\frac{S_T}{S_{ref}}\right)$
Thrust		D_T	$0.5\rho\left(V_p^2\right)S_{ref}C_{D(T)} \times \left(\frac{S_T}{S_{ref}}\right)$
T	$0.5\rho\left(V_p^2 - U_\infty^2\right)S_p$	M_T	$0.5\rho\left(V_p^2\right)S_{ref}C_{M(T)} \times \left(\frac{S_T\overline{C}_T}{S_{ref}\overline{C}_{ref}}\right) + L_T l_T$

6.2. Wind Tunnel Tests of Powered Monoplane and Biplane MAVs

In order to confirm the benefit of using the biplane concept for achieving lower-speed flights and decreasing induced drag at low speed with fixed-wing MAVs, a series of three powered models have been tested and compared. All three models are fabricated using composite fiber material. The two monoplane concepts are *MinusKiool* and the *MiniLady* (a scaled-down of the *LadyBug* which has same planform as the *Plaster*). Both monoplane powered models are equipped with one or two LRK 13-6-11Y motor and the GWS 4540 propeller in this test. The brushless motors are connected to an external electric supply installed outside the test section. The *MiniLady* is another monoplane wing similar to the *Plaster* but it is equipped with only one fixed vertical stabilizer instead of two vertical stabilizers in the *Plaster*. A pair of elevons provides control on the pitch and roll axis. The wing planform is the

Plaster wing, which is formed by joining a half-ellipse and a rounded-corner rectangle at mid chord. The wing root chord is 170 mm and the span is 240 mm so that the aspect ratio is 1.7 and a dihedral angle of 5º ensures lateral stability. The airfoil is a double-camber thin airfoil of 4mm constant thickness (about 2% relative thickness at root chord) which maximum relative camber is 3.5% at 30% chord and a negative camber of 0.9% at 76% chord.

Finally, the *TYTO20* (Fig.13) is a tandem-wing bimotor MAV which total span is 190 mm. The forewing is an inverse Zimmerman wing with a root chord of 110 mm and an aspect ratio of 2.17. The airfoil section is a 0.8mm-thick fiber-carbon cambered plate which root chord corresponds to the NACA 4412 mean camber line. The lower wing has a crescent shape which moulds the trajectory of the propeller tips and takes a full advantage of their blowing effect. Both the lower and upper wings are joined at the tips through winglets, which artificially increase the overall aspect ratio and provide additional rigidity. Finally, a horizontal tail, equipped with a pair of elevons, is located in the wake of the propellers in order to remain efficient throughout the whole flight envelope. For the powerplant, *TYTO20* is equipped with two micro-motors LRK 10-6-16Y and a pair of GWS 3030 propellers. The tests are performed at three different speeds of 5, 10 and 15 m/s. The efficiency of control surfaces of all three models was also determined and compared.

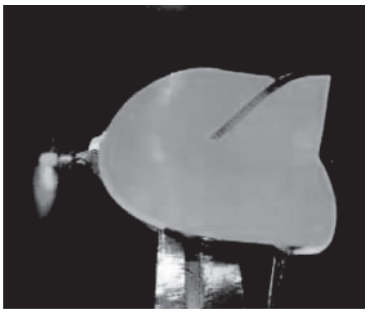

MiniLady

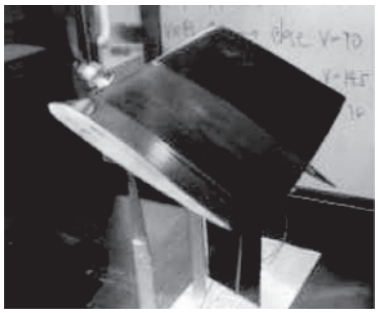

MinusKiool

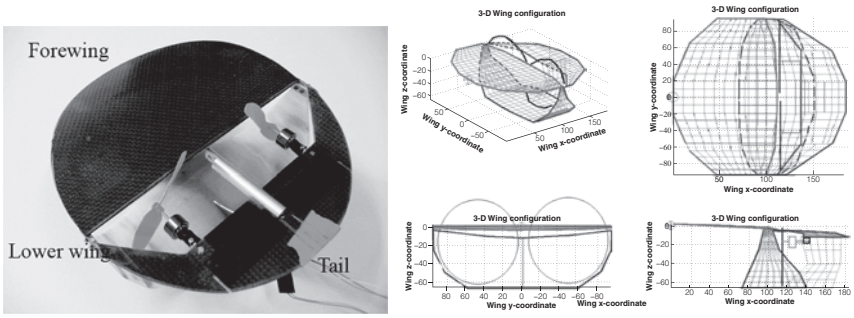

TYTO20

Figure 13. Schematic views of wind tunnel test models (monoplane & biplane).

The results are shown in Table 9. They confirm that the biplane configuration has an induced drag factor k lower than both monoplane MAVs for both unpowered and powered model cases. The minimum drag of *TYTO20* is significantly higher than that of *MinusKiool* and *MiniLady* for unpowered model nevertheless it is smaller for powered model. Using motor thrust represented in 7th column to estimate minimum of three MAVs, minimum drag of 10 Watts-Powered-MinusKiool, -MiniLady, and -TYTO20 increases approximately about 4.7, 7.2, and 2.6 times of those unpowered model. This is strongly due to propulsive tractor and pusher configuration as investigated in section 5. High increment of minimum drag compared with result in Table 7 is also responded to thick airfoil and particularly due to presence of fuselage in *MiniLady* MAV. The addition of winglets to monoplane configurations can slightly reduce the induced drag factor K as expected from the experience of classical airplane, but their efficiency proves very low at such low Reynolds numbers and is reported to decrease with the angle of attack [24]. All in all, the experimental results confirm an advantage of biplane MAV over monoplane wings with or without winglets for a typical speed lower than 10 m/s. From Table 9, it appears that at 10 m/s, without propellers in action, the *TYTO20* has the highest lift force for a maximum dimension

Table 9. Characteristics of MinusKiool, MiniLady, and TYTO20 concept at 10 m/s

MAV Model	Unpowered Model: AC; cm	CL_{max}	AoA_{stall}	K	CD_0	Powered Model (Identical Power 10 Watts): Thrust; N	w/o Winglet: K	w/o Winglet: CD_0	with Winglet: K	with Winglet: CD_0
MinusKiool	4.1	0.59	20.0º	0.37	0.039	0.60	0.35	–0.124	0.35	–0.121
MiniLady	5.2	0.47	21.5º	0.42	0.034	0.60	0.39	–0.066	0.38	–0.063
TYTO20	4.8	1.05	26.4º	0.32	0.059	0.54	0.26	–0.107	–	–

identical to monoplane MAVs. The unpowered biplane configuration produces a lift force 1.4 times higher than the best monoplane MAV, *MiniLady*. For the tandem-wing configuration, it turns out that the fore wing always stalls before the aft wing, resulting in additional safety.

Table 10 compares the performances of monoplane and biplane powered models at two different flow speed regimes, 5 m/s (low speed) and 10 m/s (cruise speed). In both cases, identical electrical inputs have been set to compare the performance of all configurations at the same total electric power (16 Watts). The voltage has been kept constant at 10.9 Volts which corresponds to a 3-cell Lithium battery and the electric current has been set to 1.47 Amps. The angle of attack is adjusted so that the lift force balances a total weight of 80 grams. At low speed, the *TYTO20* generates a maximum lift coefficient higher than both monoplane configurations and still quite far from the current lift coefficient (C_L = 1.7). It shows a positive (nose-up) pitching moment around the aerodynamic center and the drag coefficient being negative, the speed can be further reduced for the *TYTO20*, with a pitching moment at the center of gravity lower than for monoplane MAVs. For all models, the center of gravity has been placed with a static margin of 10%.

Table 10. Characteristics of powered model at identical electric input power (16 Watts)

MAV Model	Wind Speed 5 m/s: CL_{max}	AoA_{stall}	80 g–lift (CL1.7): CD	80 g–lift (CL1.7): CM_{cg}	Wind Speed 10 m/s: CL_{max}	α_{stall}	80 g–lift (CL0.42): CD	80 g–lift (CL0.42): CM_{cg}
MinusKiool	2.25	52º	–0.10	–0.30	1.15	31º	–0.08	–0.07
MiniLady	2.50	48º	0.00	–0.25	1.25	33º	–0.07	–0.08
TYTO20	2.75	48º	–0.30	–0.22	1.75	40º	–0.08	–0.10

In summary, the tandem-wing *TYTO* configuration requires less electric power to fly at low speed, produces a lower nose-down pitching moment coefficient around the center of gravity and proves capable of flying at lower speeds due to its higher maximum lift coefficient and smaller induced drag factor.

6.3. A Low-speed MAV Based on the Tandem-Wing Concept

To illustrate the tandem-wing concept, a 30 cm-span scaled-up model from *TYTO20* has been build. This model is called *TYTO30* (shown in Fig. 14) and was built by Boris Bataillé in February 2007 in view of carrying an autopilot and a video camera. The prototype has been designed to enter the MAV07 outdoor competition, which includes a series of surveillance tasks to be performed in autonomous mode. The untwisted upper wing has a thin cambered airfoil identical to the NACA4412 mean camber line with a constant thickness of 4 mm. The lower wing has flat plate airfoils and a crescent shape similar to that of the 20 cm-span model. The horizontal tail and lower wing are connected with a fixed vertical tail, which provides directional stability and enhances the overall airframe rigidity. Elevons are controlled by two servos located in the fuselage through a hollow carbon rod, which connects the upper wing and horizontal tail. Yaw can be piloted using differential thrust, which is important to conduct very low-speed flights. The *TYTO30* is compact and rigid because all three surfaces are joined at the tip in a box-wing fashion. The total weight is 230 grams, which includes 30 grams of payload (CCD video camera) and the autopilot *Paparazzi* developed by ENAC [25–26]. The autopilot, receiver and a 3-cell Lithium Polymer battery of 730 mAh are integrated in the fuselage. A 2-axis gimbaled camera platform that fits into a Ping-Pong ball is developed and placed at the nose tip. During the flight, the data can be measured by the GPS receiver and the horizon sensors are used to tilt the camera in such a

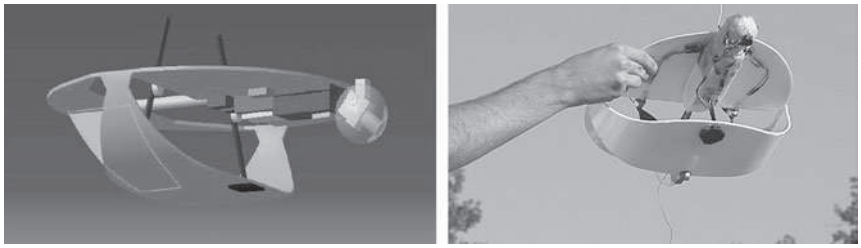

Figure 14. Schematic views of the TYTO30 (left) and the TYTO30 ready to fly (right).

way that it is continuously pointing toward an object located on the ground. Two brushless motors LRK 13-6-11Y (7.6 grams each) and two 12 cm-diameter carbon propellers of 8 cm-pitch from *Wes Technik* are installed in a pusher configuration at the upper wing trailing edge. It should be noticed that in the pusher configuration, propellers are protected during landing. The center of gravity is set to ensure a 7%-static margin. Because the horizontal stabilizer equipped with elevons is placed right behind the propellers, both pitch and roll control are guaranteed even in the low-speed regime. The direction of rotation is chosen so as to act against wing tip vortices and artificially increase the wing aspect ratio. It also favors the maneuverability since, when turning right, the left motor should speed up while the right motor should slow down to produce a yaw moment. By doing so, an induced roll moment is produced which tends to turn right. The design of new counter-rotating propellers is conducted using *XROTOR* and results in the fabrication of a pair of light carbon fiber counter-rotating propellers optimized for a cruise speed of 10.5 m/s. A new series of flight tests confirms that the use of counter-rotating propellers is essential to achieve full control in the low speed regime. Finally, in September 2007, the *TYTO30* successfully completed the MAV07 outdoor mission by ranking third out of 14 entries. Since each motor is capable of producing a static thrust of 200 grams, current studies are under way to investigate the possibility of hovering with the present tandem-wing bimotor concept.

7. CONCLUSIONS

The purpose of the present study is to assess the benefit of biplane configurations for the design of fixed-wing MAVs. Wind tunnel measurements as well as computations are extensively carried out to compare standard monoplane MAV configurations with different biplane wing combinations in the low Reynolds number regime. Different geometrical parameters such as gap, stagger, decalage angle, wing chord ratio have been analyzed both numerically and experimentally. A moderate vertical distance between the wings, a positive stagger and a slightly positive decalage angle are found to yield the best aerodynamic performances. Computations reveal that the biplane aerodynamic performances are optimized by applying chord ratio equal to 0.6. Furthermore, the propwash effect has also been carefully analyzed and several propeller-wing combinations have been compared. Propulsive pusher configuration exhibits greater efficiency for the low speed flight. In particular, when placed along the trailing edge of the upper wing, a pair of counter-rotating propellers in pusher configuration yields the best trade-off between a low minimum achievable speed and a limited electric consumption. The advantage of a biplane MAV configuration over the standard monoplane wing MAV is confirmed by a low-speed wind tunnel campaign based on several 20-cm MAV. Pusher biplane concept proves its aerodynamic performance in term of lower drag and high maximum lift comparing with tractor monoplane wing in a stringent dimension. Induced-drag is 1.5 times lower than that of monoplane MAVs due to biplane wing. Although, in unpowered MAV, biplane wing generates greater parasite drag because of boundary layer effect, the minimum drag of powered-TYTO is small since propellers are mounted at main wing trailing edge. Jointed wing design improves rigidity of thin wing structure and reduces the size of biplane. Propeller is also protected from the ground during the landing phase by lower wing. Finally, for maintaining control efficiency over the whole flight envelope, it has been proposed to design a horizontal stabilizer placed downstream the propellers in order to maintain aerodynamic efficiency through the propwash effect during low speed translations.

ACKNOWLEDGEMENTS

The present study has been partially supported by the French Ministry of Defence, under grant DGA-036000070, the French Ministry of Foreign Affairs and Kasetsart University, Thailand. This work could

not have been completed without the constant support from both parties. The authors would like to express their gratitude to Alain Combes and Paul-Claude Dufour for their assistance in the wind tunnel measurements and to Dominique Bernard and Boris BataillÎ for their valuable contribution in the design and development of biplane MAV prototypes.

REFERENCES

1. Mueller, T. J., Overview of Micro-Air-Vehicle Development, *Introduction to the Design of Fixed-Wing Micro Air Vehicles including three cases studies*, edited by Mueller, T. J., Kellogg, J. C., Ifju, P. G., and Shkarayev, S. V., AIAA Education Series, 2006, pp. 1–38.
2. Liu, T., Comparative Scaling of Flapping- and Fixed Wing Flyers, *AIAA Journal*, Vol. 44, No. 1, 2006, pp. 24–33.
3 Ifju, P. G., Albertani, R., Stanford, B. K., Claxton, D. J., and Sytsma, M. J., Flexible-Wing Micro Air Vehicle, *Introduction to the Design of Fixed-Wing Micro Air Vehicles including three cases studies*, edited by Mueller, T. J., Kellogg, J. C., Ifju, P. G., and Shkarayev, S. V., AIAA Education Series, 2006, pp. 185–240.
4. Aki, M., Waszak, M., and Shkarayev, S., Development of Micro Air Vehicles with in-Flight Adaptive Wing, *Introduction to the Design of Fixed-Wing Micro Air Vehicles including three cases studies*, edited by Mueller, T. J., Kellogg, J. C., Ifju, P. G., and Shkarayev, S. V., AIAA Education Series, 2006, pp. 241–276.
5. Isogai, K. and Harino, Y., Optimum Aeroelastic Design of a Flapping Wing, *Journal of Aircraft*, Vol. 44, No. 6, 2007, pp. 2040–2048.
6. Rakotomamonjy, T., Ouladsine, M., and Le Moing, T., Modelization and Kinematics Optimization for a Flapping-Wing Microair Vehicle, *Journal of Aircraft*, Vol. 44, No. 1, 2007, pp. 217–231.
7. Thipyopas, C. and Moschetta, J.M., From Development of Micro Air Vehicle Testing Research to the Prototype of TYTO: Low Speed Biplane MAV, *AIAA Applied Aerodynamic Conference*, AIAA paper 2008-6250, Honolulu, August 2008.
8. Mueller, T. J., Torres, G. E., and Srull, D. W., Elements of Aerodynamics, Propulsion, and Design, *Introduction to the Design of Fixed-Wing Micro Air Vehicles including three cases studies*, edited by Mueller, T. J., Kellogg, J. C., Ifju, P. G., and Shkarayev, S. V., AIAA Education Series, 2006, pp. 39–108.
9. Moschetta, J. M. and Thipyopas, C., Aerodynamic of Biplane Micro Air Vehicles, *European Micro Air Vehicle Conference and Flight Competition*, Braunschweig, 2004.
10. Moschetta, J. M. and Thipyopas, C., Aerodynamic Performance of a Biplane Micro Air Vehicle, *Journal of Aircraft*, Vol. 44, No. 1, 2007, pp. 291–299.
11. Munk, M. M., General Biplane Theory in Four Parts, *NACA Report*, No. 151, 1923.
12. Prandtl, L., Induced Drag of Multiplanes, *NACA Technical Note*, No. 182, 1924.
13. Diehl, W. S., Relative Loading on Biplane Wings of Unequal Chords, *NACA Report*, No. 501, 1935.
14. Selig, M. S., and al., *Summary of Low-Speed Airfoil Data Vol.1*, 1st Edition, SoarTech Publications, Virginia, 1995.
15. Melin,T., TORNADO: A Vortex lattice MATLAB Implementation for Linear Aerodynamic Wing Applications, *Master thesis*, Royal Institute of Technology, Dept of Aeronautics, Kungliga Tekniska Högskolan, Stockholm, 2001.
16. Suhariyono, A., Kim, J. H., Goo, N. S., Park, H. C., and Yoon, K. J., "Design of precision balance and aerodynamic characteristic measurement system for micro air vehicles", *Aerospace Science and Technology*, Vol. 10, 2006, pp. 92–99.
17. Kochersberger, K., Abe, C., "A Novel, Low Reynolds Number Moment Balance Design for Micro Air Vehicle Research," *23rd AIAA Applied Aerodynamics Conference, June 6–9, 2005, Toronto, Ontario, Canada*, AIAA paper 2005-4759, June 2005.
18. Pelletier, A. and Mueller, T. J., "Low Reynolds Number Aerodynamics of Low-Aspect-Ratio, Thin/Flat/Cambered-Plate Wings," *Journal of Aircraft*, Vol. 37, No. 5, 2000, pp. 825–832.

19. Thipyopas C. and Moschetta, J.M., Improved Performance of Micro-Air Vehicles Using Biplane Configuration, *11th Australian International Aerospace Congress*, paper WC-0120, 13–17 March 2005, Melbourne, Australia.
20. Thipyopas, C., Comparison Pusher and Tractor Propulsion for Micro Air Vehicle, *General Aviation Technology Conference & Exhibition*, paper no. 06GATC-13, Wichita, 2006.
21. Kellogg, J. C., Case Study: Micro Tactical Expendable Rigid-Wing Micro Air Vehicle, *Introduction to the Design of Fixed-Wing Micro Air Vehicles including three cases studies*, edited by Mueller, T. J., Kellogg, J. C., Ifju, P. G., and Shkarayev, S. V., AIAA Education Series, 2006, pp. 151–184.
22. Hoerner, F. H. and Borst, H. V., *Fluid-Dynamic Lift 2nd edition*, published by Hoerner, L.A. 1985, chapter 12.
23. McCormick,B.W., *Aerodynamics of V/STOL Flight*, 3rd Edition, Dower Publications, Inc., New York, 1999.
24. Viieru, D., Albertini, R., Shyy, W., and Ifju, P. G., "Effect of Tip Vortex on Wing Aerodynamics of Micro Air Vehicles," *Journal of Aircraft*, Vol. 42, No. 6, 2005, pp. 1530–1536.
25. Brisset, P., Drouin, A., Gorraz, M., Huard, P.-S., Tyler, J., "The Paparazzi Solution", *Proceedings of the 2nd US-European Competition and Workshop on Micro Air Vehicles*, (MAV'06), October 30–November 2, 2007, Sandestin, Florida.
26. Brisset, P., Drouin, A., Jestin, Y.,"Reengineering the Paparazzi Autopilot Navigation System", *6th IFAC Symposium on Intelligent Autonomous Vehicles* (IAV2007), September 3–5, 2007, Toulouse, France.